Graphene oxide enhanced nanocellulose/chitosan biodegradable aerogel pad for fresh pork preservation

Ning Zhang
Yangtze University
Xiaokang Xu
Yangtze University
Simiao Zhang
Yangtze University
Mei Zhou
Yangtze University
Yutong Huang
Yangtze University
Weiqing Sun
Yangtze University
Jing Ma
majing@yangtzeu.edu.cn
Yangtze University
Lifeng Wu
Hainan Institute for Food Control

Research Article

Keywords: Nano-cellulose, Chitosan, Graphene oxide, Aerogel pad, Pork preservation

Posted Date: February 8th, 2024

DOI: https://doi.org/10.21203/rs.3.rs-3935392/v1

Additional Declarations: No competing interests reported.

Version of Record: A version of this preprint was published at Food and Bioprocess Technology on April 25th, 2024. See the published version at https://doi.org/10.1007/s11947-024-03406-z.

Abstract

This study aimed to to prepare a degradable bacteriostatic aerogel pad that can absorb pork exudate extension for long pork shelf life. The addition of Graphene oxide(GO) was used to improve the bacteriostatic and mechanical characteristics of nanocellulose(CNC) and chitosan(CTS) matrix materials, and the bacteriostatic aerogel was obtained by freeze-drying technique. The results showed that when GO concentration was 0.4wt%, the antibacterial aerogel network had uniform structure, good mechanical properties and water/oil adsorption, and exhibited effective growth and reproduction inhibition against Escherichia coli and Staphylococcus aureus. Under the condition of 4℃, the bacteriostatic aerogel with 0.4wt% GO could be used as the packaging pad of fresh pork, absorbed the juice oozed during the storage process of pork, prolonged the fresh pork's shelf life and postponed the color, pH, and TVB-N changes.

1. Instruction

In the fresh pork storage process, in addition to the color, smell, hardness and other sensory changes, the most obvious is that there is juice oozing, these juices will not only affect the sensory evaluation of consumers on the meat, but also more likely to promote the meat breeding micro-organisms so as to speed up the rate of corruption(Wang et al., 2024). Therefore, the development of adsorbent pads is necessary in the special case of fresh meat packaging. Aerogels with large internal surface area, high porosity and uniform pore size have been the preferred choice for adsorbent materials. However, most of the materials used for the preparation of aerogels are made of chemical synthetic polymers that are difficult to degrade(Chen et al., 2022), such as polyurethanes, polyimides and polyvinylidene fluoride. These polymers are highly chemically stable, do not break down easily and can be harmful to soil, oceans and even entire ecosystems(Benito-González et al., 2020). Therefore, it has become an inevitable trend to follow the principle of sustainability and the policy of circular economy to reduce the use of chemicals and fossil energy, and to replace traditional chemically synthesised polymers with biopolymers that are rich in sources, renewable and degradable. Biodegradable biopolymers prepared from polysaccharides, proteins, lipids and other substances extracted from silk, wood and plant renewable resources, which are abundantly available in nature, have become new materials for food packaging(Júnior et al., 2014; Santillo et al., 2022). These studies show that the state of the art in biodegradable packaging has reached a point where it is promising for widespread use..

As the most numerous and abundant natural polymer material in nature, cellulose and its derivatives are widely found in hemp, cotton and wood (Zhang et al., 2018). Nanocellulose(CNC) obtained from cellulose hydrolysis has high mechanical properties, biodegradability and low density(Costa et al., 2021). It has the characteristics of stable performance and recycling, and is a valuable material for aerogel preparation for research. However, due to the high hydrophilicity of cellulose, the obtained aerogels are prone to decomposition when exposed to moisture, and thus require hydrophobic treatment(Benito-González et al., 2020). Chitin is the second largest renewable natural polymer material in nature, mainly extracted from the shells of marine crustaceans. Chitosan(CTS) obtained from chitin by deacetylation is the only positively charged polymer in natural polysaccharides(Zhang, 2021). CTS is not only biodegradable but also has good biocompatibility and bacteriostatic properties(Zhang, 2023). The positively charged CTS contains amino groups, and there are electrostatic interactions with both the negatively charged CNC and the anionic sulphate semiester groups generated during sulphuric acid hydrolysis to prepare CNC, and the ionic interactions between CTS and CNC can be used to fabricate stable three-dimensional scaffolds(Doustdar et al., 2022). Costa et al. (2021) found that the composite film formed by surface modification of CNC with CTS had enhanced tensile properties, water absorption and water vapour barrier properties; The scaffolds obtained by using CNC and CTS as matrix materials and adding $CaCl_2$ or glutaraldehyde as cross-linking agents can be completely degraded in PBS solution, which has potential bone tissue engineering applications(Doustdar et al., 2022). From the perspective of environmental protection and resource recycling, composite aerogels can be prepared by combining cellulose derivatives with chitosan for meat preservation, but the mechanical properties and bacterial inhibition of aerogels prepared in this way tend to be weak.

Graphene oxide(GO), one of the most promising nanostructures, is a two-dimensional monolayer of sp2-bonded carbon atoms with good antimicrobial and biosafety properties in addition to excellent thermal and mechanical properties. The structure of GO contains a large number of functional groups that contain oxygen., llike hydroxyl group (-OH), carboxyl group (-OH), and

epoxy (-CH(O)CH-), which make GO hydrophilic, and stable chemical bonds can be formed with the polymer molecules, which ensures good compatibility between GO and hydrophilic polymers(Li et al., 2022; Yang et al., 2019). In previous studies, GO doping has successfully enhanced the properties of various types of polymers, for example, gelatin(Maryam Adilah et al., 2022), chitosan(Yadav & Ahmad, 2015), polylactic acid (Zhao et al., 2022). Wu et al. (2023)'s study showed that starch/chitosan films modified with carboxymethylcellulose-modified graphene oxide can be used to preserve fruit, Arfat et al. (2018) and Maryam Adilah et al. (2022) similarly suggested that composites containing graphene oxide have potential for food packaging applications.Studies on compostability and biodegradability(Cruz et al., 2023; Han Lyn et al., 2019) have shown that GO/polymer films decomposed down in soil burial tests.

In this research, GO was doped into CNC/CTS aerogels, CNC/CTS/GO antibacterial aerogels were prepared by freeze-drying technique, and the attributes of the aerogel were characterised, and the effect of the aerogel mat on fresh pork preservation and its biodegradability were further analysed.

2. Materials and methods

2.1 Instruments and materials

Microcrystalline cellulose(MCC), CTS(degree of deacetylation ≥ 95%, viscosity: 100-200mpa.s, Mw = 1,000,000)and GO(sheet size: 0.5–1.5μm, thickness: 1-3nm) from Sinopharm Chemical Reagent Co., Ltd. were acquired. Every chemical was graded as an analytical reagent. Sample preparation was done using deionized water.

2.2 Preparation of CNC/CTS/GO aerogels

CNC was obtained by hydrolysis of MCC using sulphuric acid, which was configured into a 6wt% aqueous solution and ultrasounded until completely dissolved for use. Dissolved CTS powder in 2wt% acetic acid and stirred until dissolved to obtain 4wt% CTS solution and set aside. Added the GO powder to ultra-pure water, ultrasounded until the GO powder was completely dissolved, get the GO water solution, set aside. The three solutions were added to the reaction bottle and stirred in the water bath for 3h to obtain the mixed solution, which was packed in the 24-well plate. Pre-frozen at -80℃ for at least 3h, then freeze-dried at -60℃ for 48h, to obtain CNC/CTS/GO antibacterial aerogel(Fig. 1).

2.3 Characterization of CNC/CTS/GO aerogels

The aerogel samples' infrared spectra were recorded within the scope of 500–4000 cm-1 using an IR-960 Fourier transform infrared spectrometer (FT-IR) (Tianjin Rui Bank Technology Co., Ltd.).

The dried aerogels were sticked to the sample table with conductive adhesive, and the scanning electron microscope was used to the sample surfaces. (VEGA3.TESCAN) at 20 kV with a magnification of 100×.

Each aerogel's weight was determined by an analytical balance, and measured the diameter by vernier caliper and measuring the height at three different positions. Aerogel density was calculated from Eq. (1). where *v* represented the aerogel sample's volumetric weight and *m* was weight.

Density = $\frac{m}{v}$ (1)

Aerogels' porosity was measured by liquid replacement method. Ethanol was chosen as an alternative liquid because it can easily pass through the pores without causing structural changes in the samples. Furthermore, the sample was insoluble in ethanol. The sample (*W1*) was weighed and immersed in ethanol for 5 minutes, subsequently the sample was removed and weighed (*W2*). The porosity ε was computed using the subsequent Eq. (2) (Doustdar et al., 2022).

$$\epsilon = \frac{w2 - w1}{\rho_{eth} \times V_{scaffold}}$$

2

The mechanical properties of the dried aerogels were measured at room temperature using a TA-XT Plus mass tester (Stable Micro Systems, UK). The test rate was 60 mm/min; compression deformation was 70%; test speed was 1.0 mm/s; and a cylindrical acrylic probe (P/36R) with a diameter of 36 mm. All measurements were made in at least triplicates.

Placing the aerogel sample in distilled water or peanut oil, removed periodically, weighed after removing excess liquid from the surface, and the process was repeated until the sample mass reached equilibrium and the amount adsorbed per gram of sample was calculated. After equilibrium, the samples were dried under ambient conditions until the weight was constant (about 24 hours) and the water/oil adsorption was calculated from Eq. (3), where *Wd* and *Ww* denoted the weights of the samples prior to and following the water/oil absorption test. The mass of the sample after 24 hours and the starting mass of the sample at equilibrium were used to compute the retention capacity of water and oil, as shown in Eq. (4) (Chatterjee et al., 2020), where W_{24h} is the sample's mass following the water or oil absorption and leaving it at 25°C for 24 hours, and W_{0h} was the mass of the sample after saturating with water/oil.

water/oil adsorption capacity(g/g) = $(W_w - W_d)/W_d$ (3)

Water and oil retention capacity(%)=$(W_{24h} - W_w)/(W_{0h} - W_w)$ (4)

The samples were weighed *(W1*) and soaked in distilled water at ambient temperature, after 24 hours the samples were removed from the water, the water was wiped off the surface of the samples and the weight (*W2*) was measured. The degree of swelling (*WSD*) was calculated by Eq. (5).

WSD=((W2 − W1)/W1)×100% (5)

Turbidimetric method was used to measure the bacterial inhibition rate of the aerogel(Wu et al., 2023). The bacterial suspension with the aerogel sample added was used as the experimental group and the suspension without the sample added was used as the blank control group. The bacteria were shaken at 37°C and 200 rpm for 2, 4, 6 and 8 h. The OD value of the bacterial solution at each time point was determined at 600 nm using a visible spectrophotometer. The antibacterial characteristics of the aerogels were quantitatively characterized by calculating the average value of three trials conducted for each group.

The matrix soil was mixed proportionally with vermiculite to evaluate the degradability of the aerogel and Bacillus subtilis solution was added to speed up the degradation process. The test conditions were room temperature 25°C and soil relative humidity 95%, after 10, 20 and 30 days, the biogels were removed, washed and dried until the quality of the aerogels did not change anymore. The biodegradation rate was assessed according to the Eq. (6), where m_f denotes the weight of the aerogel after oven drying (g) and m_i is the starting weight of the aerogel (g)(Yang et al., 2022).

Biodegradation rate(%)=$((m_f - m_i)/m_i)\times 100\%$ (6)

2.5 CNC/CTS/GO aerogel pad for fresh pork preservation

The purpose of the preservation studies was to evaluate the ability of GO-0.4 antibacterial aerogel to preserve fresh pork(Zeng et al., 2022). Simply, fresh pork was selected and separated into three groups. The control group was placed directly in the tray and the experimental group was filled with trays of composite aerogel pads (GO-0) and antimicrobial aerogel pads (GO-0.4), respectively, and stored at 4°C. Physico-chemical parameters of fresh pork samples were determined on days 0, 2, 4, 6, 8, 9, 10, 11, 12 and 13.

L*(brightness), a*(red/green) and b*(yellow/blue) values for fresh pork samples, used Minolta Laboratory colorimeter (CM-5, Minolta Camera Corporation, Osaka, Japan)(Duran et al., 2016)

The sample mass *M1* before storage and *M2* after storage were accurately weighed, and the mass loss was calculated according to Eq. (7).

$$\textit{Mass loss(\%)} = \frac{|M1 - M2|}{M1} \times 100\% \quad (7)$$

The method of Chen et al. (2022) was utilized for measureing the pH of pork samples.

TVB-N content was an indicator of meat freshness, according to the standard NP-1848-1987, measured by microdiffusion method(Costa et al., 2021).

2.6. Statistical analysis

Graphs were plotted with the aid of Origin 2021. (OriginLab Co., Northampton, MA), the mean and standard deviation of the data were reported, using SPSS 25.0 software(SPSS Inc., Chicago, IL), one-way analysis of variance (ANOVA) was used to analyze significant differences ($P < 0.05$).

3. Results and discussion

3.1 Characterization of CNC/CTS/GO aerogel

The surface morphology of the antibacterial aerogels were seen with the use of scanning electron microscopy, as depicted in **Fig.2A**. There was a three-dimensional mesh structure in every aerogel sample., and the size of the aerogels' pores gradually decreased and converged with the rise in GO addition. When the GO was not added, hydrogen bonds were formed between CNC and CTS through electrostatic interactions, and there was obvious aggregation in the aerogel, which was attributed to the fact that CNC was easy to self-assemble in the polymer matrix to form coarse aggregates without GO. When GO was added, in addition to the formation of hydrogen bonds between CNC and CTS(Chaichi et al., 2023), there was a reduction in the formation of CNC aggregates due to the two-dimensional planes of GO that can absorb compatible nanomaterials as well as the similar oxy-surface functionality of CNC and GO, which promotedd the formation of many cross-links between them (Santillo et al., 2022). Moreover, the reaction of the carboxyl groups of GO with the amino groups of CTS to form hydrogen bonds also enhanced the structure of the aerogel (Gong et al., 2019), which tended to stabilize and homogenize the aerogel's three-dimensional network.

The aerogel prepared with the addition of GO was extremely lightweight and it can stand on a dandelion as shown in **Fig.2B**. The density of antibacterial aerogel with added GO was significantly higher than that of composite aerogel without added GO (**Fig.2C**). There wasn't a noticeable variation in the density increase when the addition amount is 0.2wt% ~ 0.4wt%. When the GO concentration reached 0.8wt%, the aerogel density was about twice as high as that without GO addition. On the one hand, this was because of the formation of strong hydrogen bonding interactions between GO and the CNC/CTS polymer chains(Gong et al., 2019), which acted as an auxiliary, which was consistent with the SEM results. On the other hand, this was due to the fact that GO hada certain mechanical strength and that GO was homogeneously embedded in the polymer network structure, avoiding severe volume shrinkage. (Ashiri & Mehdipour, 2018).

The more pores, the greater the specific surface area, which means that aerogels have more active surfaces with higher adsorption capacity. This gave aerogels important applications in adsorption and catalysis. **Fig.2D** showed the porosity of aerogels with different concentrations of GO added, it can be seen that the porosity of the aerogel demonstrated a propensity to rise before falling with the increase of GO concentration, and the porosity of the aerogel was the largest when the concentration is 0.2wt%, which indicated that at this time, the framework of the aerogel was the most equilibrium with the porosity.The smaller porosity when the concentration of GO was low was due to the self-assembling behaviour of the CNCs to form aggregates (Santillo et al., 2022); At high concentrations, the smaller porosity may be due to the saturation of GO, where GO nanosheets that did not form hydrogen-bonded connections attach to occupy the empty area created by the polymer chains, and the pore size decreased (Li et al., 2022).

3.2 Mechanical properties of aerogels

The aerogel samples' stress-strain curves (**Fig.3**) can be categorized into the subsequent phases. The stress and strain in the first stage are linear because the stress was small, the curve was relatively flat, at this time the aerogel produced an elastic shape, with the contraction of the aerogel, the stress gradually increased. In the second stage, it should be under higher strain, the curve gradually changed from linear to non-linear, and the aerogel started to deform. In the third stage, the curve stabilises after the aerogel specimen reached the yield stress and the plastic deformation produced during this phase further caused the aerogel structure to collapse. In the final stage, the stress increases dramatically, the pore volume was compressed, and the aerogel's initially porous, loose three-dimensional network structure became dense.

The compressive strength of the aerogel samples with different GO concentrations varied significantly and as the concentration of GO rose, the compressive strength also increased. Moreover, at an addition concentration of 0.4 wt%, the aerogel was capable of carrying a maximum weight of 180 g without damaging its shape or appearance(**Fig.3**). This phenomenon occurred because increasing the content of GO as a reinforcing material increases the strength of the aerogel structure (Wu et al., 2023). The hydroxyl groups of CNC and the amine groups of CTS can interact to form effective hydrogen bonds. With the increase of GO content, the aerogels with GO added had better mechanical properties than those without GO due to the hydrogen bonding between CNC and GO, suggested that GO acted as a reinforcing phase. Another study showed that the amide groups formed by the reaction of CTS with the carboxyl groups of GO increased the degree of fibre entanglement and thickened the surface of the samples due to the addition of GO. Therefore, it was experimentally demonstrated that GO formed stable and uniform cross-links with CNC and CTS, which improved the mechanical properties of the aerogel.

3.3 Swelling capacity of aerogels

As the GO concentration increased from 0 to 0.8wt%, the colour of the aerogel gradually changed from the white colour of GO itself to brown (**Fig.4A**). The aerogel samples were immersed in water for 24 hours to confirm the water stability of the aerogels through the dissolution and swelling of the aerogels. When the dry aerogel came into touch with water, it absorbs the water readily and creates hydrate, which led to the expansion of the aerogel structure, and the color gradually changed to dark brown, but the aerogel still maintained its original morphology for a long time in the water. (**Fig.4B**). As soon as the water absorption force and retention force reached a balance, the aerogel reaches the maximum water absorption force. If the water absorption persisted, the structure of the aerogel will be damaged (Wang et al., 2024). **Table 1** illustrated that with the rise in GO concentration, the degree of swelling of the aerogel increased and then decreased. When the concentration of GO is 0.4wt%, the swelling degree reached the maximum, indicating that the structure of GO-0.4 aerogel is more stable, which is related to the increase in the degree of fibre entanglement after the addition of GO. At this time, the water molecules entering and leaving the internal channels of the aerogel sample reached equilibrium, consistent with the adsorption of water/oil by the aerogel.

Table.1 Swelling degree of GO aerogels with different concentrations(0, 0.1wt%, 0.2wt%, 0.4wt%, 0.8wt%) and after dissolution (B).

GO concentration	GO-0	GO-0.1	GO-0.2	GO-0.4	GO-0.8
Swelling capacity	2323.138±181.65C	2630.76±117.944AB	2523.37±67.55B	2713.97±35.22A	2583.88±177.42AB

Notes: The values are mean ± SD of three deviations. Different letters “A, B, C” in the same column indicate significant differences ($P < 0.05$).

3.4 Water/oil adsorption and desorption capacity and retention rate of aerogels

As shown in **Fig.5**, the aerogels had excellent oil and water absorption. After the addition of GO, the aerogels' capacity to absorb both water and oil with 0.2wt% and 0.4wt% GO were changed to different degrees, and the water absorption and oil absorption of the aerogels showed an increasing trend. This occurred as a result of GO's addition, the aerogel pad reformed a more ordered porous structure that was more conducive to the adsorption of water and oil(Yang et al., 2019). However, when the addition amount reached 0.8wt%, part of the GO existed in the aerogel pad in the way of filling, but affected the entry and exit of water and oil, which also explained the higher water retention rate of GO-0.8 aerogel. In addition, after CNC, CTS and GO were combined, the combination of hydroxyl and carboxyl groups reduced the hydrophilic groups on the surface of CNC and GO, and the hydrophilicity decreased(Wang et al., 2014). The oil retention rate of all aerogels was close to 100%, and there was no significant reason mainly because the viscosity of the oil was larger, and the volatile temperature of the oil was as high as 190℃, and the loss was very small at 25℃.

3.5 FT-IR of aerogels

The FT-IR spectra of CNC, CTS, GO, CNC/CTS aerogel, and CNC/CTS/GO aerogel were shown in **Fig.6**. CNC/CTS/GO aerogel had stretching vibrations of -OH and N-H at 3200-3450 cm^{-1}, C=O stretching at 1643 cm^{-1}, stretching vibrations of carboxyl groups at 1053 cm^{-1}, and amide group hydroxyl groups at 1643 cm^{-1}. Compared to the CNC/CTS aerogel, the characteristic peaks of CNC and GO were not well discerned due to the overlap of the characteristic peaks associated with CTS, but the appearance of the amide group peak at 1643 cm^{-1} and the increase in the intensity of the carbonyl peak at 1628 cm^{-1} were due to the increase in the carbonyl group concentration upon the incorporation of CTS and the formation of amide groups by reacting with GO, which demonstrates that the GO has formed crosslinks with CNC
and CTS(Gong et al., 2019).

3.6 Antibacterial activities of aerogels

The growth curves of Staphylococcus aureus and Escherichia coli were displayed in **Fig.7**, it went to show that the OD values of E. coli and Staphylococcus aureus grew steadily over with incubation period. After adding aerogel samples, OD values of Staphylococcus aureus and Escherichia coli decreased significantly, and OD values of bacteria decreased with the increase of GO concentration. This was because both CTS and GO have antibacterial ability, and the antibacterial mechanism of chitosan was mainly the electrostatic interaction between its positive charge and microbial cell membrane with a negative charge, which led to the intracellular component leaking and resulted in the demise of cells. However, the positive charge of chitosan in GO-0 aerogel and the negative charge of CNC generated electrostatic interaction, resulted in a large reduction of positive charge, and the antibacterial effect was not obvious(Costa et al., 2021). The bacteriostatic mechanism of GO was the direct contact between GO and bacteria, and the RNA of the bacterium was destroyed by the membrane tension that GO's sharp edge causes(Cao et al., 2022). When the GO concentration was higher, the antibacterial effect was better. It could also be seen from **Fig.7** that the inhibition effect of aerogel samples on Staphylococcus aureus was stronger than that of E. coli, that was because the difference in cell wall structure between the two bacteria. While Staphylococcus aureus had a thicker cell wall than E. coli, since it lacked an outer membrane, direct contact interactions are difficult for it to withstand. When GO concentration is 0.4wt% and 0.8wt%, there was no significant difference in the inhibition effect of aerogels on Escherichia coli. Therefore, combining the results of solubility and water-oil adsorption, we chose GO concentration of 0.4wt% to prepared antibacterial composite aerogels for the following experiment.

3.7 Analysis of the effect of pork preservation

As the duration of storage increased, the quality loss rate of all pork samples showed an increasing trend (**Fig.8A**). This was because tissue shrinkage caused by the influence of external environment during storage was caused by the loss of moisture in the pork itself, as well as the loss of nutrients, resulting in the reduction of pork quality(Wang et al., 2024). The mass loss

rate of the GO-0 and GO-0.4 groups was higher than that of the blank control group, mainly because of the high adsorption capacity of the aerogel pad, which could quickly absorb the juice of the pork and prevent the existence of the juice from providing favorable conditions for the reproduction of microorganisms.

From day 0 to day 13, the color of pork in all groups changed from bright red to dark red, and the surface of pork in the blank group had obvious moisture, and the color was darker than that in the other two groups（**Fig.8B**）. The values of L* (brightness), a* (red/green) and b* (yellow/blue) were indicators to evaluate the color of pork. The values of L* (**Fig.8C**), a* (**Fig.8D**) and b* (**Fig.8E**) all exhibited a declining trend as the amount of time spent storing pork increased, which was because myoglobin in muscle was oxidized to oxygenated myoglobin after contact with air. With the extension of muscle contact time with oxygen, oxygenated myoglobin was gradually oxidized to high ferrimyoglobin, giving meat a dark brown color. The content of oxygenated myoglobin decreased after oxidation, and the color of pork gradually turned yellow(Xi et al., 2023).

Fig.9A displayed the variation of pH value of pork with varying storage times. With the extension of storage time, all samples exhibited a trend of initially dropping and then increasing. The pH of all samples on day 3 was lower than at the time of slaughter because the initial drop in pH was likely due to the accumulation of inorganic phosphoric acid brought on by the depletion of muscular adenosine triphosphate (ATP) depletion and the breakdown of glycogen to produce lactic acid(Lan et al., 2016). After the fourth day, the pH of pork began to gradually increase, mainly due to the degradation of proteins by meat spoilage microorganisms and endogenous enzymes to produce ammonia, amines and other basic substances, which gradually accumulated as storage duration increases(Xu et al., 2023). The normal range of pH value: 24 h after slaughter pH value is 5.45~5.80, the pH value of ordinary fresh pork is 5.8~6.2, the pH value of secondary fresh meat is 6.3~6.7, and the pH value of rotten meat is above 6.7(Chen et al., 2022). As seen in **Fig.9A**, the pH of the samples in the blank group exceeded the normal range of fresh meat pH on day 9, while the pH of the samples in the GO-0 and GO-0.4 groups exceeded the normal range later than that of the blank group, suggesting that the use of the aerogel pads effectively delayed the deterioration of pork. This indicateed that the use of aerogel pads was effective in delaying the deterioration of pork, while the pH of the samples from the GO-0.4 group reached the limit of spoilage only after 12 days, indicating that the addition of GO produced favorable results for the extension of the shelf-life of pork.

Fresh pork should be less than 15 mg/100 g, sub-fresh meat range of 15 mg/100 g~25 mg/100 g, more than 25 mg/100 g has lost food value(Costa et al., 2021). The TVB-N of all pork samples (**Fig.9B**) showed an increasing trend during storage, which caused by the pork in microorganisms and protein enzymes, and the protein decarboxylated and deammoniated reactions, resulting in alkaline substances such as amines and nitrogen(Wan et al., 2020). The content of these substances also had a great impact on the freshness of pork(Bai et al., 2023). It can be seen that the TVB-N value of the blank group increased most rapidly, reaching the range of secondary meat on the 9th day and corrupting on the 10th day, and the GO-0 group reached the range of sub-fresh meat on the 11th day, while the samples of the GO-0.4 group reached the range of sub-fresh meat three days later than the blank group. The outcomes demonstrated that the adding of GO significantly extended the shelf life of pork.

3.8 Biodegradability of aerogel

Biodegradability test is a crucial instrument to evaluate the environmental compatibility of prepared materials. The GO-0.4 aerogel sample was biodegraded by soil burial degradation for 30 days. As shown in **Fig.10**, after soaking in soil for 30 days, the weight was reduced by 51%, a result consistent with other studies on the degradation of nanofiber wikis(Dong et al., 2023). The findings indicated that even though adding GO enhanced the antibacterial ability of the aerogel, the aerogel material still had biodegradable behavior, which may be related to simulated environmental effects in the soil, such as humidity, different types of microorganisms, and temperature(Abou Hammad et al., 2019).

4. Conclusions

This study confirmed that the CNC/CTS aerogel added with GO has antibacterial effect and can be used as a liner for fresh meat. The CNC/CTS/GO aerogel pad was prepared by freeze-drying. The results demonstrated that the aerogel exhibited good mechanical properties and water/oil adsorption when GO concentration was 0.4wt%, and had good inhibition effect on Staphylococcus aureus and Escherichia coli. The antibacterial aerogel pad prepared by adding 0.4wt% GO can extend the shelf life of fresh pork at 4℃.

Declarations

Funding

This study was financially supported by the Key Laboratory of Tropical Fruits and Vegetables Quality and Safety for State Market Regulation (KF-2023005).

Author Contribution

Ning Zhang: conceptualization, software, methodology, investigation, writing—original draft, writing—review, and editing; Xiaokang Xu: methodology, supervision, review, and editing; Simiao Zhang: supervision, investigation, project consultant, writing—review, and editing; Mei Zhou: investigation, writing—review, and editing; Yutong Huang: software, investigation, supervision; Weiqing Sun: supervision and editing;Jing Ma (Corresponding author): project consultant, methodology, investigation, writing—review, and editing; Lifeng Wu: investigation and project consultation. The present study is approved by all authors.

Data availability

Data will be made available on request.

Declaration of competing interest

The authors declare that they have no known competing financial interests or personal relationships that could have appeared to influence the work reported in this paper.

References

1. Abou Hammad, A. B., Abd El-Aziz, M. E., Hasanin, M. S., & Kamel, S. (2019). A novel electromagnetic biodegradable nanocomposite based on cellulose, polyaniline, and cobalt ferrite nanoparticles. *Carbohydrate Polymers*, *216*, 54-62. https://doi.org/10.1016/j.carbpol.2019.03.038
2. Arfat, Y. A., Ahmed, J., Ejaz, M., & Mullah, M. (2018). Polylactide/graphene oxide nanosheets/clove essential oil composite films for potential food packaging applications. *International Journal of Biological Macromolecules*, *107*, 194-203. https://doi.org/10.1016/j.ijbiomac.2017.08.156
3. Ashiri, S., & Mehdipour, E. (2018). Preparation of a novel palladium catalytic hydrogel based on graphene oxide/chitosan NPs and cellulose nanowhiskers. *RSC Adv*, *8*(57), 32877-32885. https://doi.org/10.1039/c8ra06623j
4. Bai, J., Li, M., & Cui, L. (2023). Study on bacteriostasis and preservation effectiveness of poly (vinyl alcohol) /Portulaca oleracea extract fresh□keeping films for pork. *CHINA PLASTICS*, *37*(04), 46-52. https://doi.org/10.19491/j.issn.1001-9278.2023.04.008
5. Benito-González, I., López-Rubio, A., Gómez-Mascaraque, L. G., & Martínez-Sanz, M. (2020). PLA coating improves the performance of renewable adsorbent pads based on cellulosic aerogels from aquatic waste biomass. *Chemical Engineering Journal*, *390*. https://doi.org/10.1016/j.cej.2020.124607
6. Cao, J., He, G., Ning, X., Chen, X., Fan, L., Yang, M., . . . Cai, W. (2022). Preparation and properties of O-chitosan quaternary ammonium salt/polyvinyl alcohol/graphene oxide dual self-healing hydrogel. *Carbohydr Polym*, *287*, 119318. https://doi.org/10.1016/j.carbpol.2022.119318

7. Chaichi, M., Badii, F., Mohammadi, A., & Hashemi, M. (2023). Novel Bioactive Composite Films Based on Pectin-Nanocellulose-Synergistic Triple Essential Oils: Development and Characterization. *Food and Bioprocess Technology*, *16*(8), 1794-1805. https://doi.org/10.1007/s11947-023-03036-x
8. Chatterjee, S., Ke, W.-T., & Liao, Y.-C. (2020). Elastic nanocellulose/graphene aerogel with excellent shape retention and oil absorption selectivity. *Journal of the Taiwan Institute of Chemical Engineers*, *111*, 261-269. https://doi.org/10.1016/j.jtice.2020.04.020
9. Chen, L., Niu, X., Fan, X., Liu, Y., Yang, J., Xu, X., . . . Feng, X. (2022). Highly absorbent antibacterial chitosan-based aerogels for shelf-life extension of fresh pork. *Food Control*, *136*. https://doi.org/10.1016/j.foodcont.2021.108644
10. Costa, S. M., Ferreira, D. P., Teixeira, P., Ballesteros, L. F., Teixeira, J. A., & Fangueiro, R. (2021). Active natural-based films for food packaging applications: The combined effect of chitosan and nanocellulose. *Int J Biol Macromol*, *177*, 241-251. https://doi.org/10.1016/j.ijbiomac.2021.02.105
11. Cruz, R., Nisar, M., Palza, H., Yazdani-Pedram, M., Aguilar-Bolados, H., & Quijada, R. (2023). Development of bio degradable nanocomposites based on PLA and functionalized graphene oxide. *Polymer Testing*, *124*. https://doi.org/10.1016/j.polymertesting.2023.108066
12. Dong, Y., Xie, Y., Ma, X., Yan, L., Yu, H.-Y., Yang, M., . . . Jia, B. (2023). Multi-functional nanocellulose based nanocomposites for biodegradable food packaging: Hybridization, fabrication, key properties and application. *Carbohydrate Polymers*, *321*. https://doi.org/10.1016/j.carbpol.2023.121325
13. Doustdar, F., Olad, A., & Ghorbani, M. (2022). Effect of glutaraldehyde and calcium chloride as different crosslinking agents on the characteristics of chitosan/cellulose nanocrystals scaffold. *Int J Biol Macromol*, *208*, 912-924. https://doi.org/10.1016/j.ijbiomac.2022.03.193
14. Duran, M., Aday, M. S., Zorba, N. N. D., Temizkan, R., Büyükcan, M. B., & Caner, C. (2016). Potential of antimicrobial active packaging 'containing natamycin, nisin, pomegranate and grape seed extract in chitosan coating' to extend shelf life of fresh strawberry. *Food and Bioproducts Processing*, *98*, 354-363. https://doi.org/10.1016/j.fbp.2016.01.007
15. Gong, Y., Yu, Y., Kang, H., Chen, X., Liu, H., Zhang, Y., . . . Song, H. (2019). Synthesis and Characterization of Graphene Oxide/Chitosan Composite Aerogels with High Mechanical Performance. *Polymers (Basel)*, *11*(5). https://doi.org/10.3390/polym11050777
16. Han Lyn, F., Chin Peng, T., Ruzniza, M. Z., & Nur Hanani, Z. A. (2019). Effect of oxidation degrees of graphene oxide (GO) on the structure and physical properties of chitosan/GO composite films. *Food Packaging and Shelf Life*, *21*. https://doi.org/10.1016/j.fpsl.2019.100373
17. Júnior, A. V., Fronza, N., Foralosso, F. B., Dezen, D., Huber, E., dos Santos, J. H. Z., . . . Quadri, M. G. N. (2014). Biodegradable Duo-functional Active Film: Antioxidant and Antimicrobial Actions for the Conservation of Beef. *Food and Bioprocess Technology*, *8*(1), 75-87. https://doi.org/10.1007/s11947-014-1376-9
18. Lan, Y., Shang, Y., Song, Y., & Dong, Q. (2016). Changes in the quality of superchilled rabbit meat stored at different temperatures. *Meat Sci*, *117*, 173-181. https://doi.org/10.1016/j.meatsci.2016.02.017
19. Li, T., Su, Y., Wang, D., Mao, Y., Wang, W., Liu, L., & Wen, S. (2022). High antibacterial and barrier properties of natural rubber comprising of silver-loaded graphene oxide. *Int J Biol Macromol*, *195*, 449-455. https://doi.org/10.1016/j.ijbiomac.2021.12.029
20. Maryam Adilah, Z. A., Han Lyn, F., Nabilah, B., Jamilah, B., Gun Hean, C., & Nur Hanani, Z. A. (2022). Enhancing the physicochemical and functional properties of gelatin/graphene oxide/cinnamon bark oil nanocomposite packaging films using ferulic acid. *Food Packaging and Shelf Life*, *34*. https://doi.org/10.1016/j.fpsl.2022.100960
21. Santillo, C., Wang, Y., Buonocore, G. G., Gentile, G., Verdolotti, L., Kaciulis, S., . . . Lavorgna, M. (2022). Hybrid Graphenene Oxide/Cellulose Nanofillers to Enhance Mechanical and Barrier Properties of Chitosan-Based Composites. *Front Chem*, *10*, 926364. https://doi.org/10.3389/fchem.2022.926364
22. Wan, J., Pei, Y., Hu, Y., Ai, T., Sheng, F., Li, J., & Li, B. (2020). Microencapsulation of Eugenol Through Gelatin-Based Emulgel for Preservation of Refrigerated Meat. *Food and Bioprocess Technology*, *13*(9), 1621-1632. https://doi.org/10.1007/s11947-020-02502-0

23. Wang, G., Xu, C., Zhu, S., Xu, Z., & Xiong, X. (2014). Preparation and Characterization of Graphene Oxide/Nano Cellulose Composite Film. *Packing Engineering*, *35*, 1-7. https://doi.org/10.19554/j.cnki.1001-3563.2014.13.001
24. Wang, S., Wang, F., Lu, C., Ma, S., Gu, Y., & Wang, L. (2024). Citral-loaded nanocellulose/sodium alginate aerogel packaging liner for fresh pork preservation. *Food Control*, *155*. https://doi.org/10.1016/j.foodcont.2023.110031
25. Wu, L., Lv, S., Wei, D., Zhang, S., Zhang, S., Li, Z., . . . He, T. (2023). Structure and properties of starch/chitosan food packaging film containing ultra-low dosage GO with barrier and antibacterial. *Food Hydrocolloids*, *137*. https://doi.org/10.1016/j.foodhyd.2022.108329
26. Xi, X., Hu, Y., Zhang, S., Song, Q., Huang, X., Jin, Y., . . . Hu, B. (2023). Preservation effect of nutmeg essential oil/HP-β-CD inclusion complex on chilled pork *Food and Fermentation Industries*, 1-12. https://doi.org/10.13995/j.cnki.11-1802/ts.035203
27. Xu, Y., Wen, X., Zhang, D., Schroyen, M., Wang, D., Li, X., & Hou, C. (2023). Changes in the Freshness and Bacterial Community of Fresh Pork in Controlled Freezing Point Storage Assisted by Different Electrostatic Field Usage Frequencies. *Food and Bioprocess Technology*. https://doi.org/10.1007/s11947-023-03180-4
28. Yadav, M., & Ahmad, S. (2015). Montmorillonite/graphene oxide/chitosan composite: Synthesis, characterization and properties. *International Journal of Biological Macromolecules*, *79*, 923-933. https://doi.org/10.1016/j.ijbiomac.2015.05.055
29. Yang, M., Tseng, Y., Liu, K., Cheng, Y., Chen, W., Chen, W., . . . Liu, T. (2019). Preparation of Amphiphilic Chitosan–Graphene Oxide–Cellulose Nanocrystalline Composite Hydrogels and Their Biocompatibility and Antibacterial Properties. *Applied Sciences*, *9*(15). https://doi.org/10.3390/app9153051
30. Yang, Z., Shen, C., Rao, J., Li, J., Yang, X., Zhang, H., . . . Chen, K. (2022). Biodegradable gelatin/pullulan aerogel modified by a green strategy: Characterization and antimicrobial activity. *Food Packaging and Shelf Life*, *34*. https://doi.org/10.1016/j.fpsl.2022.100957
31. Zeng, H., Hao, H., Wang, X., & Shao, Z. (2022). Chitosan-based composite film adsorbents reinforced with nanocellulose for removal of Cu(II) ion from wastewater: Preparation, characterization, and adsorption mechanism. *Int J Biol Macromol*, *213*, 369-380. https://doi.org/10.1016/j.ijbiomac.2022.05.103
32. Zhang, L. (2021). *Investigation of Multifunctional Food Packing Film via Loading Graphene Oxide onto the Procyaninids-Grafted-Chitosan Substrate* [Doctor, Tianjing University of Science and Technology].
33. Zhang, T., Zhang, Y., Wang, X., Liu, S., & Yao, Y. (2018). Characterization of the nano-cellulose aerogel from mixing CNF and CNC with different ratio. *Materials Letters*, *229*, 103-106. https://doi.org/10.1016/j.matlet.2018.06.101
34. Zhang, Y. (2023). *Preparation of Chitosan-Cod Skin Protein Hydrolysate Composite Film and Application in Pork Preservation* [Mater, Liaoning University].
35. Zhao, Y., Miao, Z., Zhang, Y., He, Z., Wang, H., & Zhao, Y. (2022). Synthesis of polylactic acid/graphene oxide composites and its properties *New Chemical Materials*, *50*(11), 83-86. https://doi.org/10.19817/j.cnki.issn1006-3536.2022.11.016

Figures

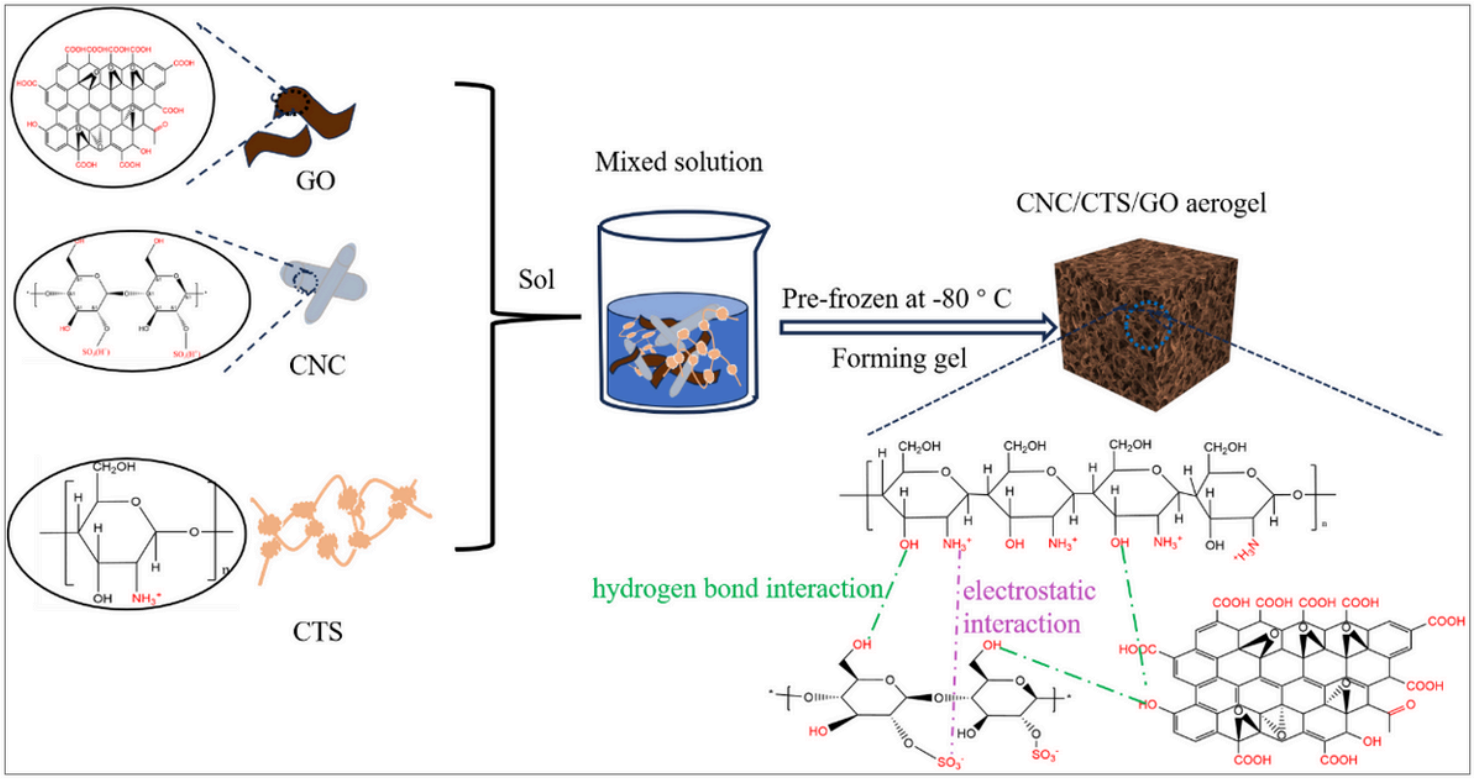

Figure 1

Schematic diagram of the synthesis method of CNC/CTS/GO antibacterial aerogel

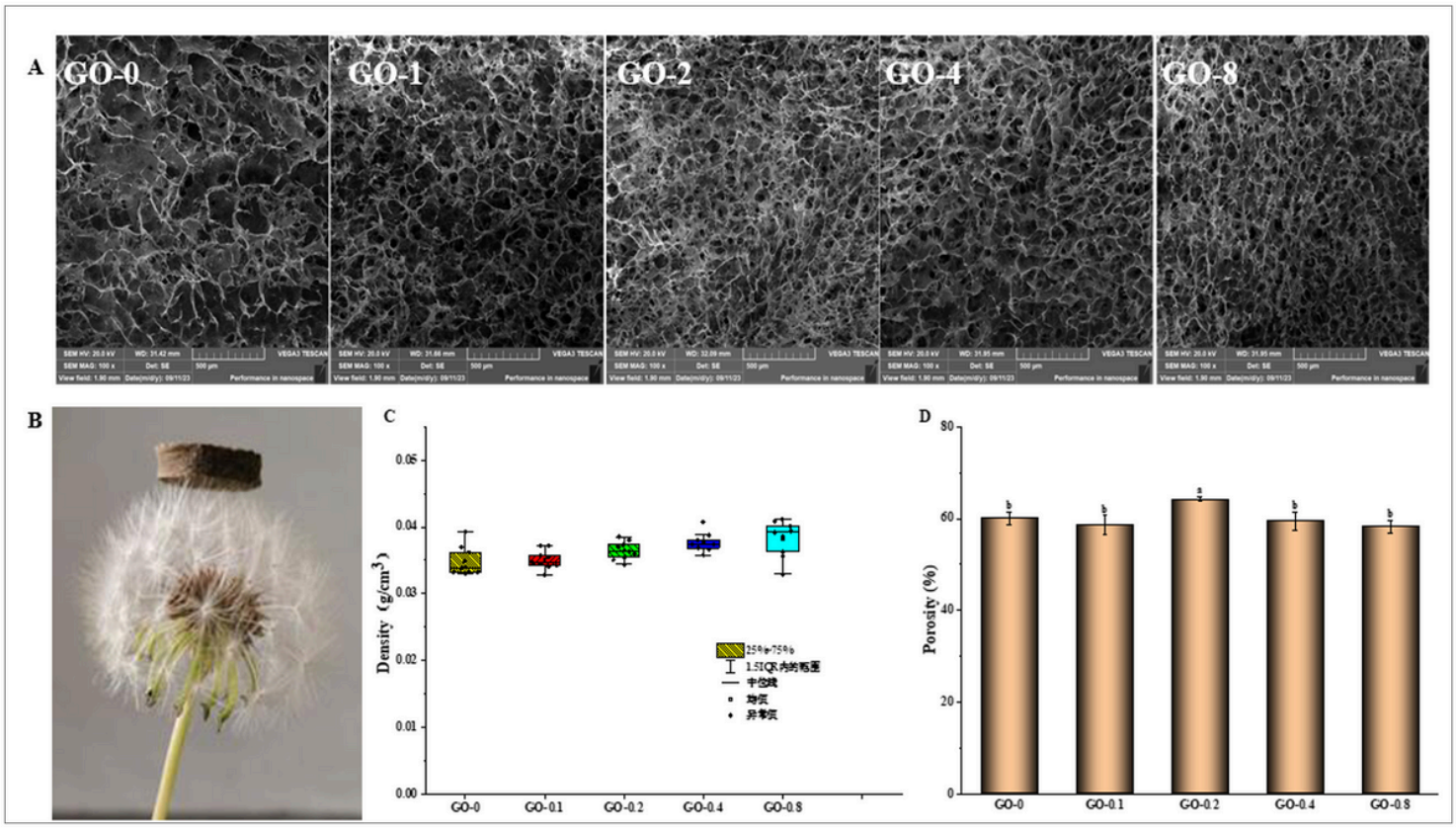

Figure 2

SEM images(A), the aerogel stands on dandelion(B), Density(C) and porosity(D)of aerogels with different concentrations of GO (0, 0.1wt%, 0.2wt%, 0.4wt%, 0.8wt%)

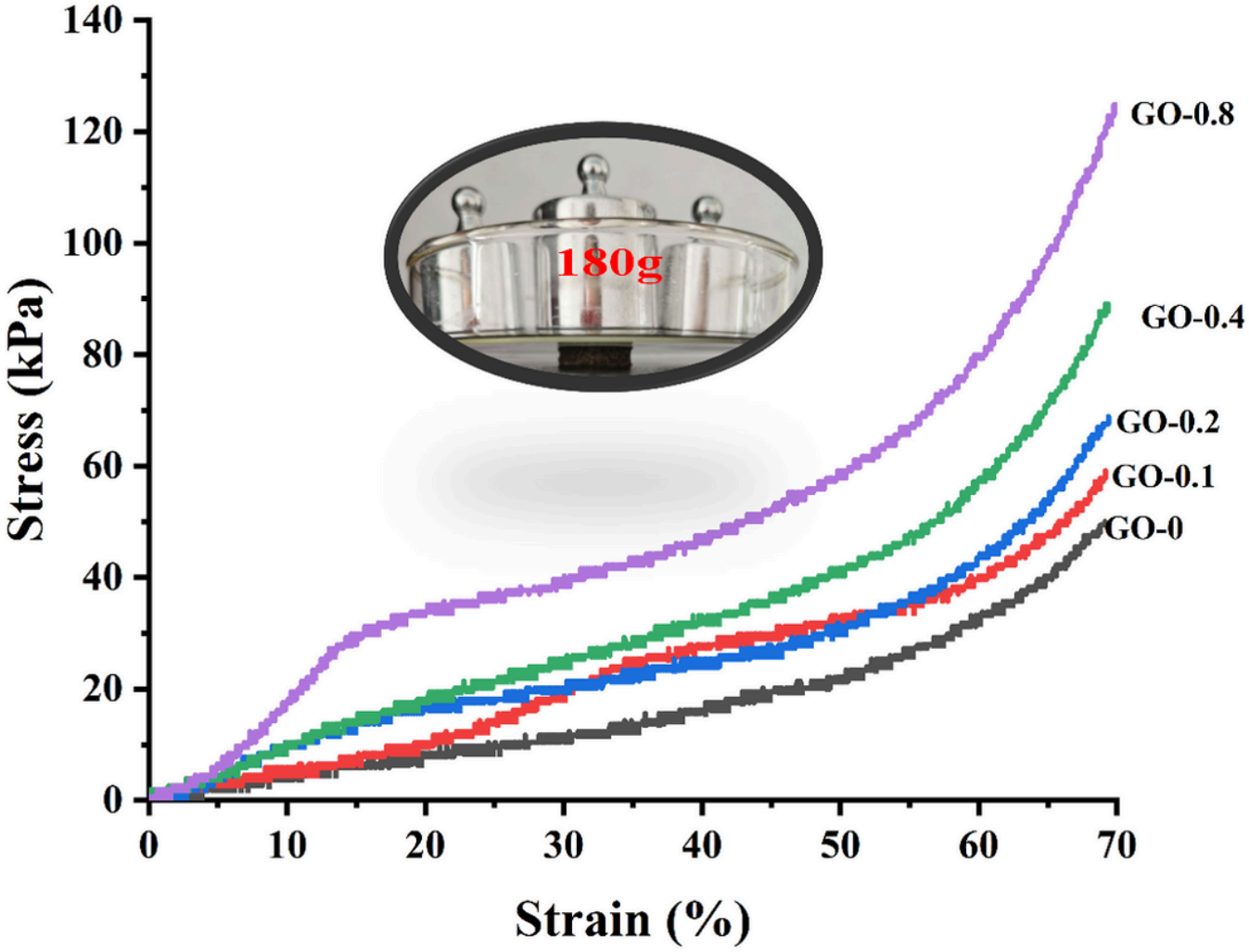

Figure 3

Stress-strain curves of aerogels with different concentrations of GO(0, 0.1wt%, 0.2wt%, 0.4wt%, 0.8wt%)

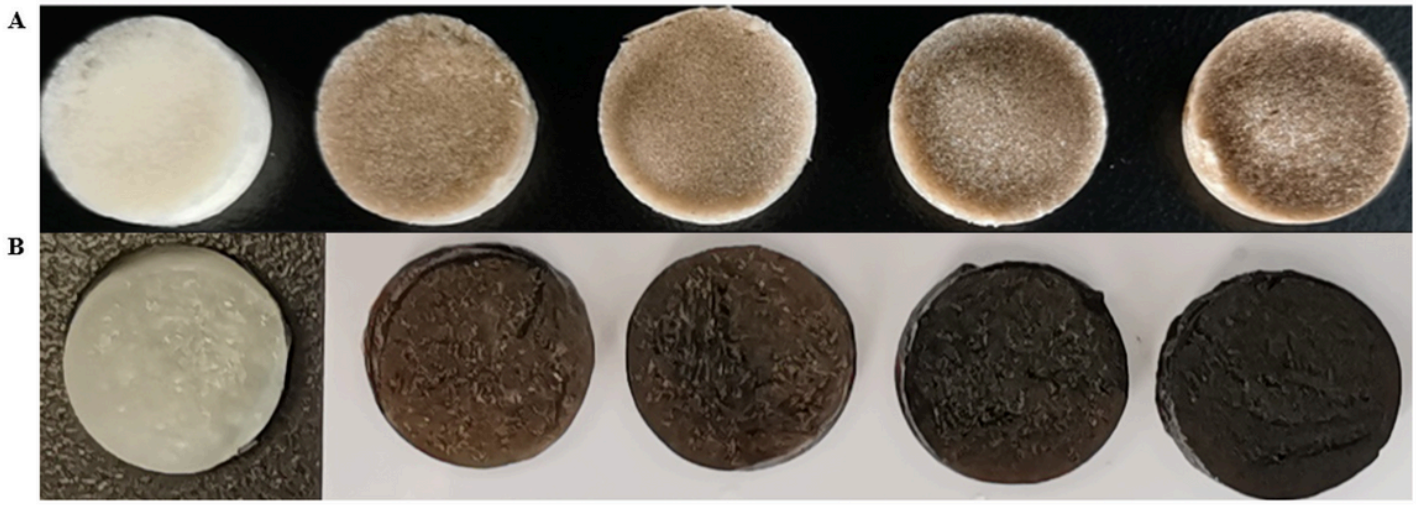

Figure 4

Visual picture(A) of GO aerogels with different concentrations(0, 0.1wt%, 0.2wt%, 0.4wt%, 0.8wt%) and after dissolution (B).

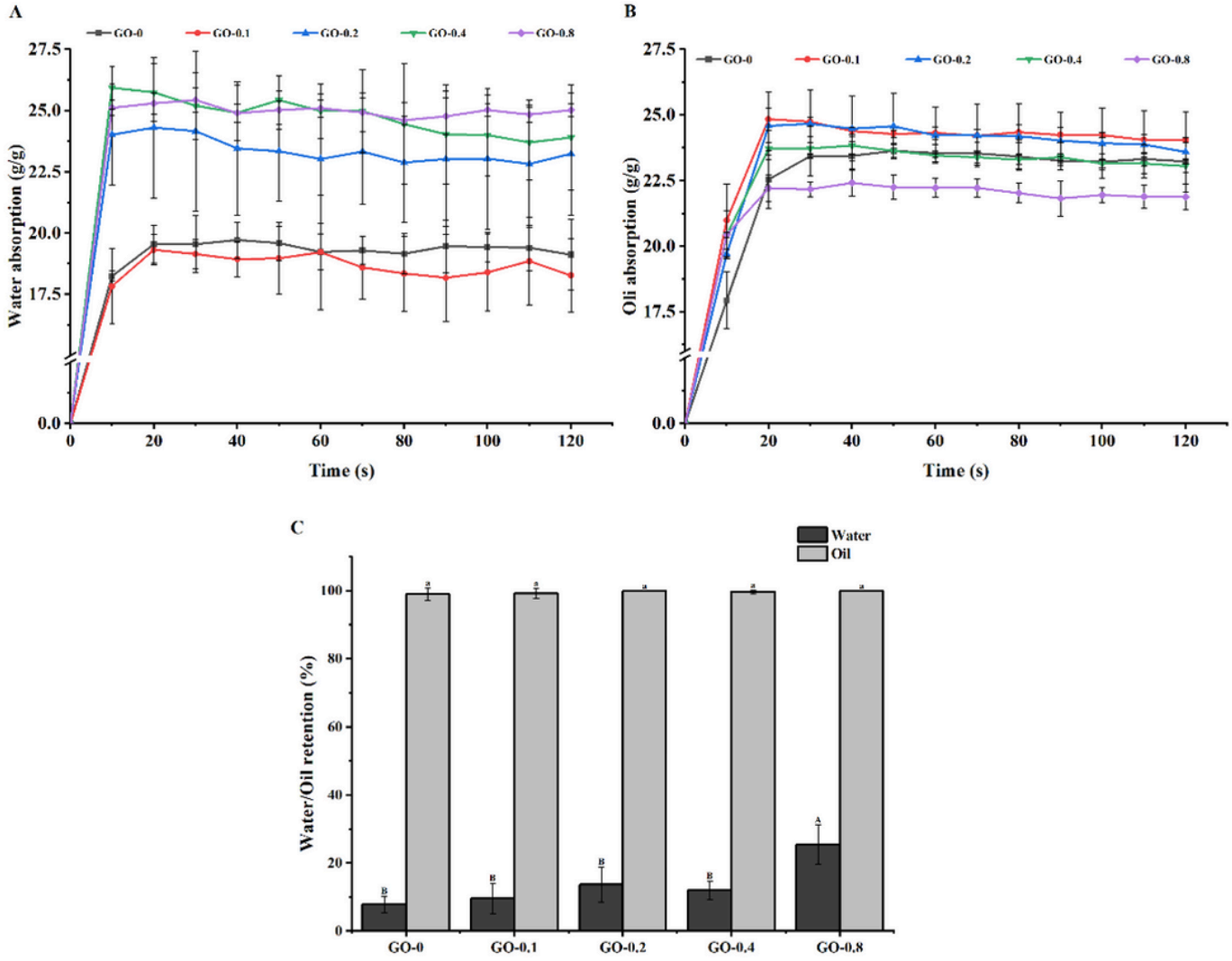

Figure 5

Water adsorption (A) and oil adsorption (B) capacities and retention rates (C) of aerogels with different concentrations of GO (0, 0.1wt%, 0.2wt%, 0.4wt%, 0.8wt%)

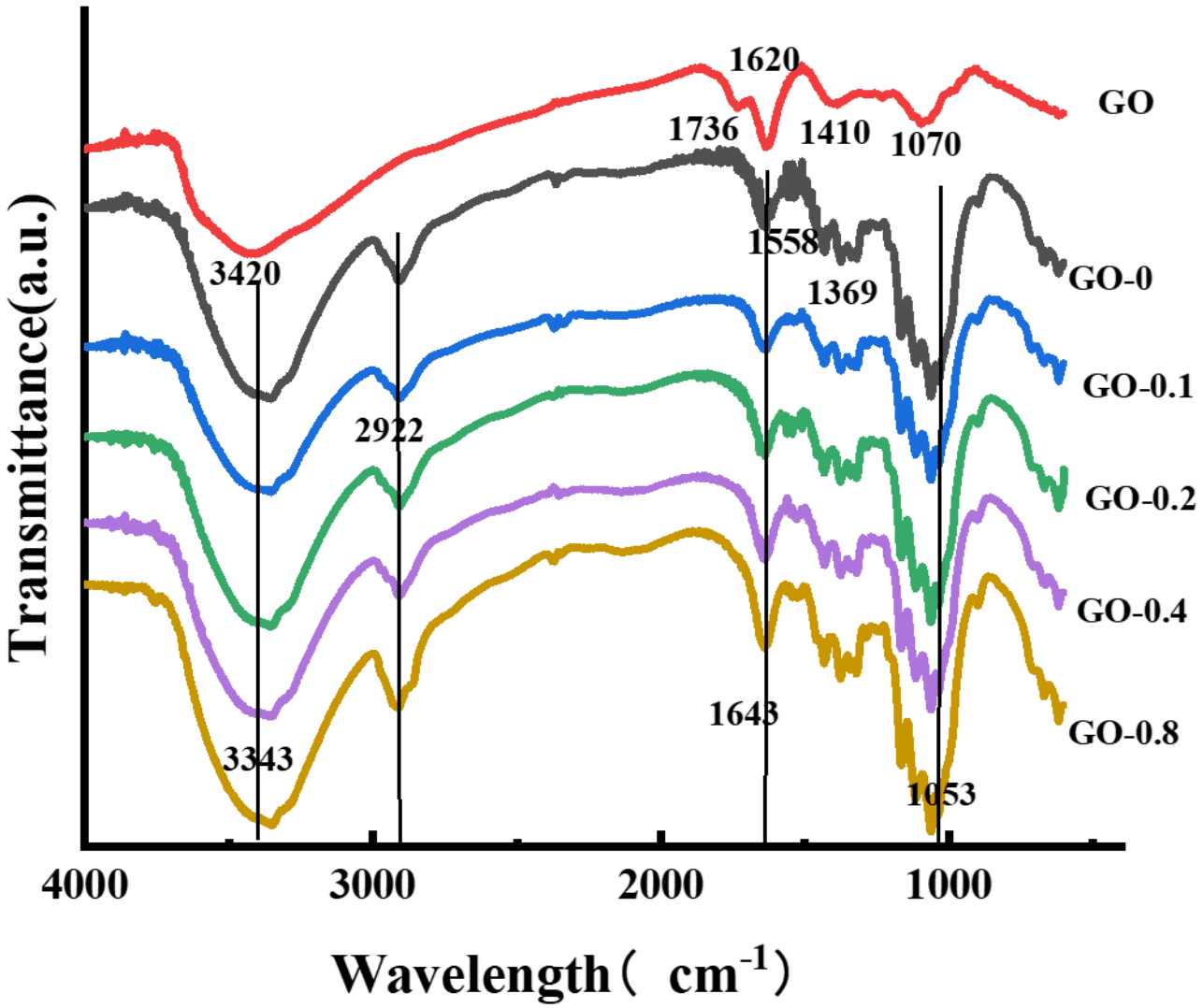

Figure 6

FT-IR spectra of aerogels with different concentrations of GO (0, 0.1wt%, 0.2wt%, 0.4wt%, 0.8wt%)

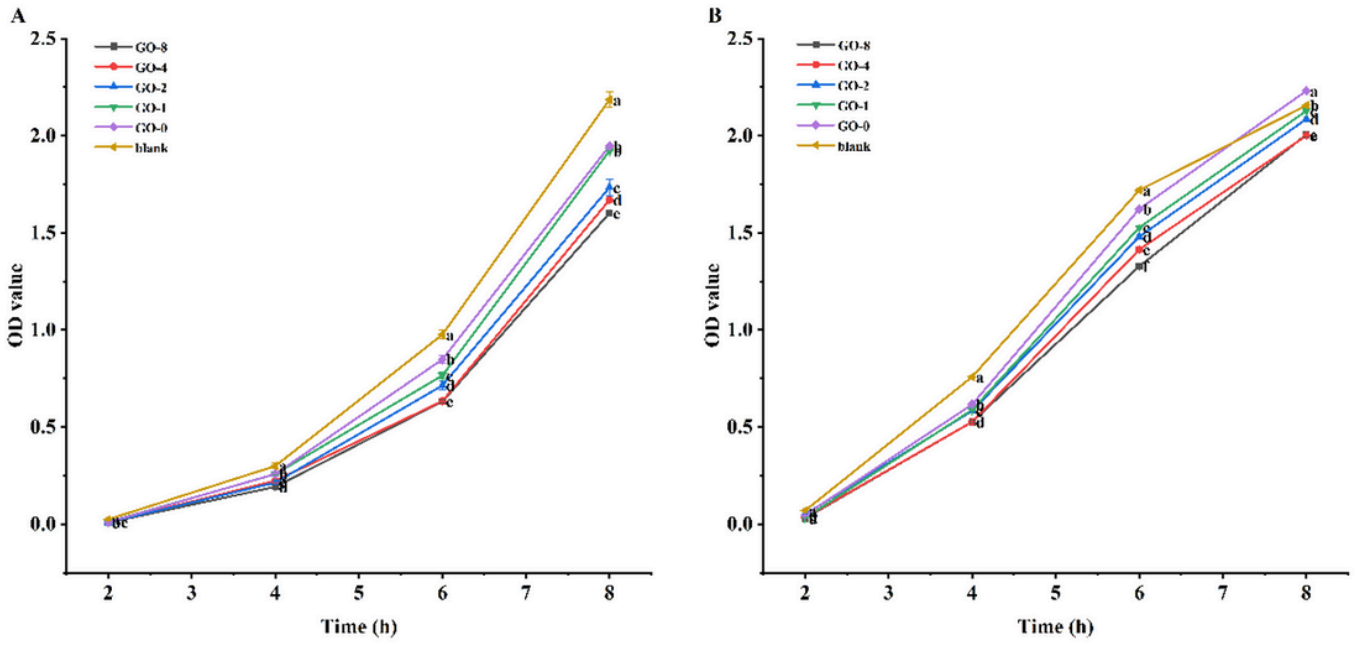

Figure 7

Growth inhibition curves of S.aureus (A) and E.coli (B) by adding aerogel with different concentrations of GO (0, 0.1wt%, 0.2wt%, 0.4wt%, 0.8wt%)

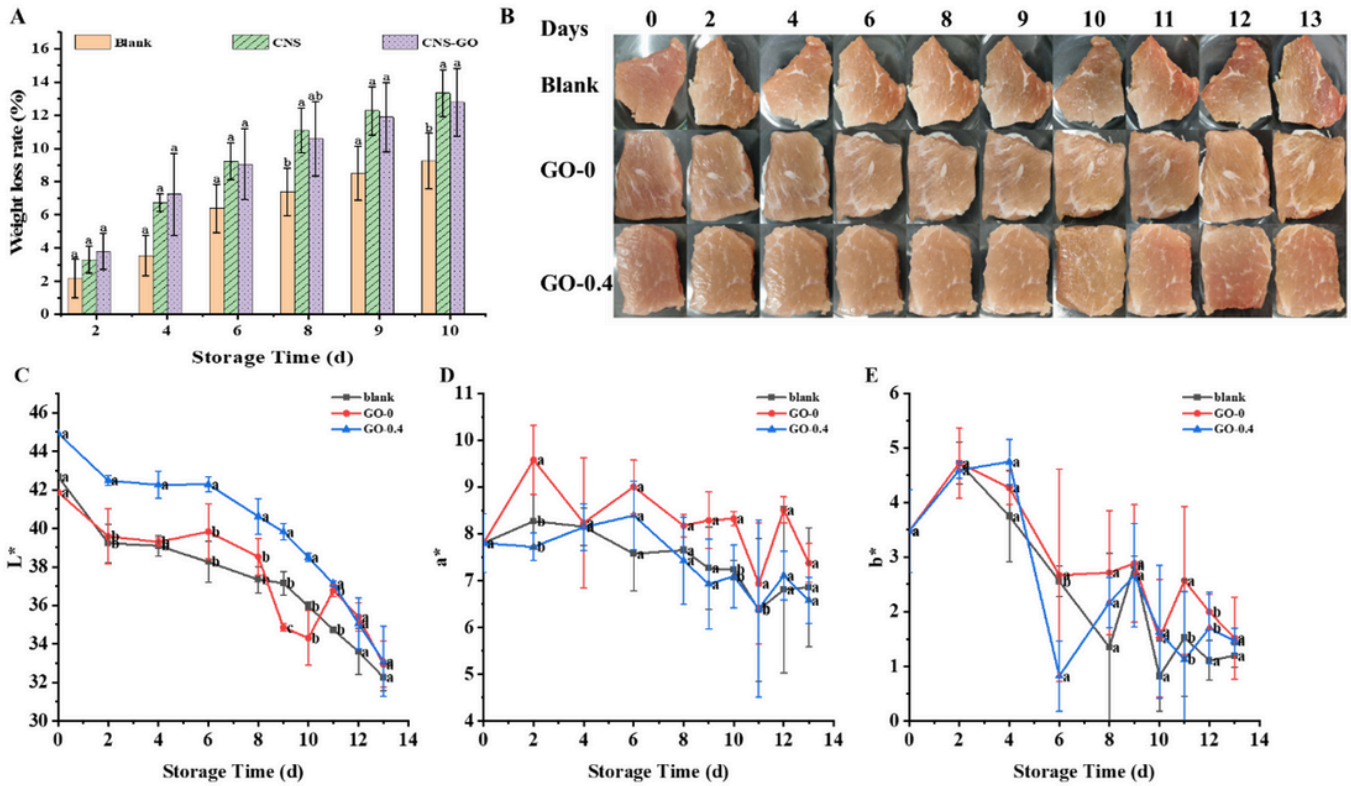

Figure 8

Masst loss rate (A), appearance (B), L* (C), a* (D)and b* (E) of pork samples during storage period

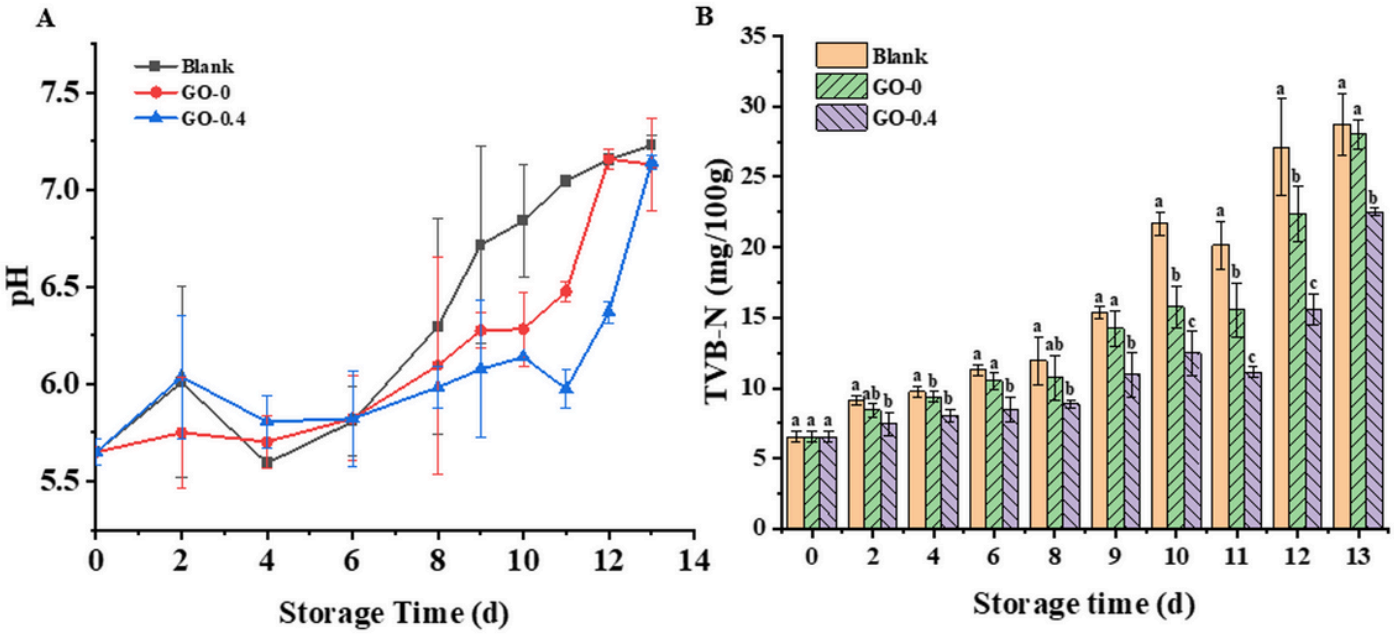

Figure 9

pH (A) and TVN-N (B) of pork samples during storage period

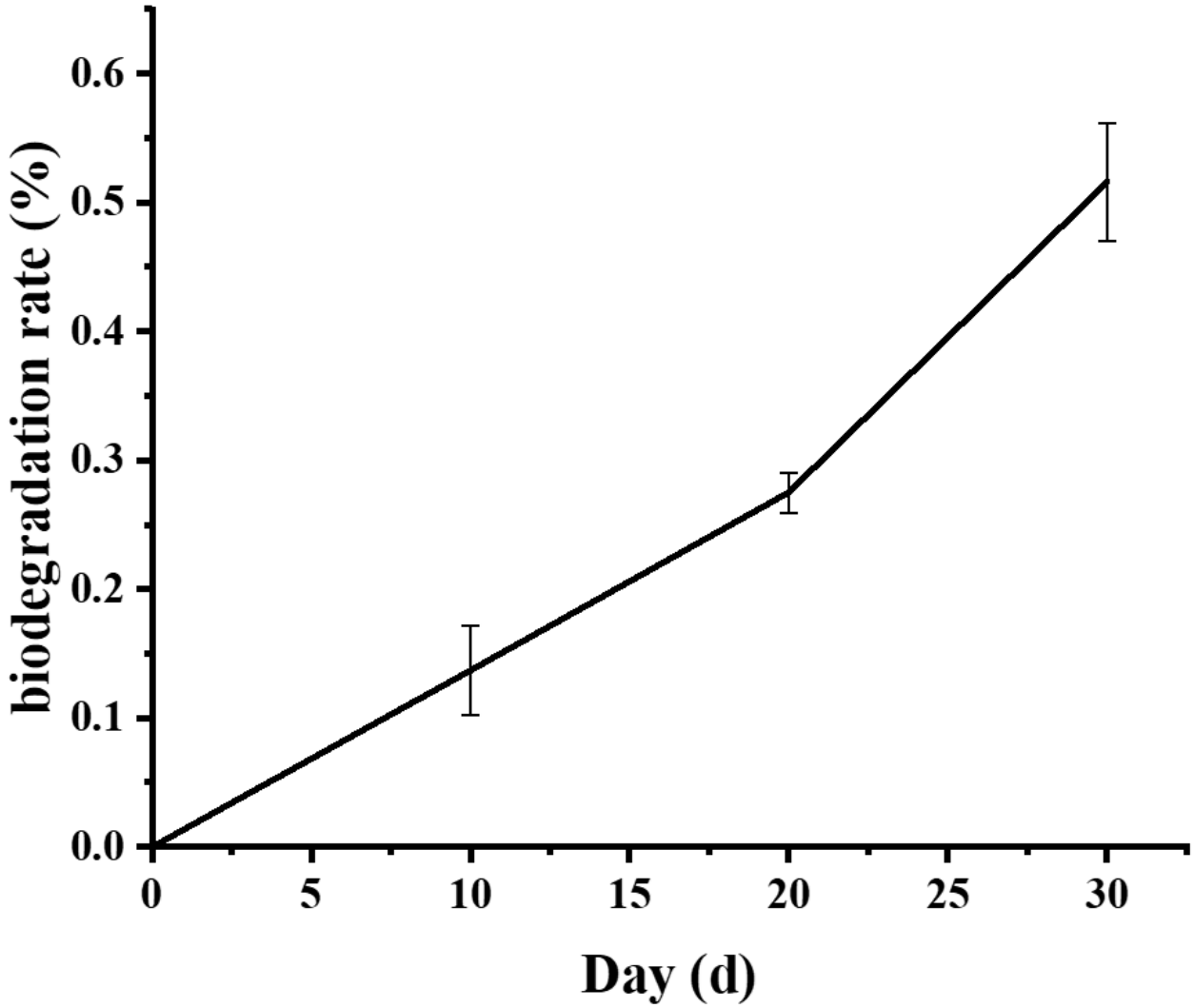

Figure 10

Biodegradation rate of GO-0.4 aerogel sample in soil